J. Fluid Mech. (2009), *vol.* 623, *pp.* 375–385.
doi:10.1017/S002211200800551X Printed in the United Kingdom

Stratorotational instability in Taylor–Couette flow heated from above

M. GELLERT† AND G. RÜDIGER

Astrophysikalisches Institut Potsdam, An der Sternwarte 16, D-14482 Potsdam, Germany

(Received 2 September 2008 and in revised form 3 December 2008)

We investigate the instability and nonlinear saturation of temperature-stratified Taylor–Couette flows in a finite height cylindrical gap and calculate angular momentum transport in the nonlinear regime. The model is based on an incompressible fluid in Boussinesq approximation with a positive axial temperature gradient applied. While both ingredients, the differential rotation as well as the stratification due to the temperature gradient, are stable themselves, together the system becomes subject of the stratorotational instability and a non-axisymmetric flow pattern evolves. This flow configuration transports angular momentum outwards and will therefore be relevant for astrophysical applications. The belonging coefficient of β viscosity is of the order of unity if the results are adapted to the size of an accretion disk. The strength of the stratification, the fluid's Prandtl number and the boundary conditions applied in the simulations are well suited too for a laboratory experiment using water and a small temperature gradient around 5 K. With such a set-up the stratorotational instability and its angular momentum transport could be measured in an experiment.

1. Introduction

In recent years instabilities in stratified media has become of greater interest. In view of astrophysical objects especially, the inclusion of stratification is relevant. One simple model to study stratification effects is the classical Taylor–Couette (TC) system. Thorpe (1968) found only a stabilizing effect of stratification. In the context of stratorotational instability (SRI), stratification in TC flows is investigated numerically with a fixed axial temperature gradient in a linear analysis studying the suppression of the onset of Taylor vortices by Boubnov *et al.* (1996). With a fixed density gradient, Molemaker, McWilliams & Yavneh (2001), Yavneh, McWilliams & Molemaker (2001) and Shalybkov & Rüdiger (2005) show the onset of a linear instability and the growth of non-axisymmetric modes. Experiments using artificially enlarged buoyancy due to salt concentration (see Withjack & Chen 1974; Boubnov, Gledzer & Hopfinger 1995; LeBars & LeGal 2006) are in very good agreement with the linear results. Caton, Janiaud & Hopfinger (2000) use an artificial diffusivity in the continuity equation and also show the results of the linear stability analysis for a non-rotating outer cylinder. Umurhan (2006) examines SRI analytically, especially the influence of vertically changing buoyancy frequency, in the quasi-hydrostatic semi-geostrophic limit. The author also shows that SRI survives only in the presence of no-slip radial boundary conditions. In the context of accretion disks, Dubrulle *et al.* (2005) figure out stability conditions and the influence of viscous dissipation and thermal diffusivity.

† Email address for correspondence: mgellert@aip.de

In particular, they find that the Prandtl number dependence of the critical parameters is unimportant. But fully nonlinear three-dimensional simulations do not exist. It is the aim of the first part of this paper to describe the characteristics of SRI in the nonlinear regime. The easiest way to do nonlinear simulations is to apply an axial temperature gradient, where the top of the TC system has a higher temperature than the bottom. The absence of a diffusivity in the continuity equation makes nonlinear simulations with explicit density gradient more demanding and favours a temperature gradient. Moreover, this is interesting from an astrophysical viewpoint: accretion disks are heated from the central object at their top and bottom. Thus the TC system heated from above could be seen as a simplified model for half of a disk. Of major interest for accretion or protostellar disks is the problem of angular momentum redistribution. Accretion works only if angular momentum is transported outwards effectively. Angular momentum transport of SRI is the second aspect of this work.

2. Model

The SRI is investigated in a model where stratification is due to a temperature gradient. Surprisingly, this gradient is positive, i.e. the cylindrical gap is heated from above. This configuration, opposite to the negative gradient in Rayleigh–Bénard systems, is perfectly stable. The second ingredient in our model is differential rotation. The inner and outer cylinders rotate with different angular velocities. Both are chosen to be positive, i.e. they exhibit the same direction of rotation. If the outer cylinder rotates sufficiently slow, the flow without temperature gradient leads to the well-known Taylor vortices for high enough Reynolds numbers. Beyond the Rayleigh line, when the outer cylinder rotates fast enough, the system is hydrodynamically stable. The combination of both stable parts can again drive the system to be unstable and generate a new instability, the SRI.

Stratification is measured by the Froude number

$$Fr = \Omega_{in}/N, \tag{2.1}$$

the ratio between angular velocity of the inner cylinder and stratification given by the buoyancy frequency

$$N^2 = \alpha g \frac{\partial T}{\partial z}. \tag{2.2}$$

Here α and g are the coefficient of volume expansion and gravity, respectively, and T is the temperature.

For computations we fix the Froude number Fr, the cylinder height and the Prandtl number. Rüdiger & Shalybkov (2008) show that moderate stratifications are the most effective. This means that the instability is suppressed for too strong stratifications as well as for too low values. For the latter in the limit $Fr \to \infty$ the instability disappears in favour of the hydrodynamically stable configuration. Hence rotation and stratification of the same order, i.e. $Fr \approx 1$, appear to be a good choice to excite the instability. Rüdiger & Shalybkov (2008) found the optimum at $Fr = 1.4$, which is well suited also for the nonlinear simulations presented here to get the smallest critical Reynolds numbers.

From an astrophysical point of view one of the most interesting questions which arises is whether the SRI can transport angular momentum. If the normalized Reynolds stress $Q_{R\phi}/(R_{in}\Omega_{in})^2$, where R_{in} and Ω_{in} are the inner radius and its angular velocity in cylindrical coordinates (R, ϕ, z), respectively, defined by the

velocity fluctuations correlation

$$Q_{R\phi} = \langle U'_R U'_\phi \rangle, \tag{2.3}$$

turns out to be positive, then angular momentum is transported outwards. This astrophysically important situation always appears to be true in our simulations, as we show in § 5. Fluctuating quantities are defined as deviations from the azimuthally averaged mean field, i.e. $\boldsymbol{U}' = \boldsymbol{U} - \langle \boldsymbol{U} \rangle$ with

$$\langle \boldsymbol{U} \rangle = \frac{1}{2\pi} \oint \boldsymbol{U} \, \mathrm{d}\phi. \tag{2.4}$$

Based on the idea that angular momentum transport is mainly enhanced via an increase in viscosity, Shakura & Sunyaev (1973) introduce in a parameterized model for a disk a coefficient

$$\alpha_{SS} = \frac{Q_{R\phi}}{H^2 \Omega_{in}^2}, \tag{2.5}$$

with the density scale height H of the disk. If the value of the α_{SS} is of the order of unity, the angular momentum transport is considered to be very effective and important. Taking the normalized Reynolds stress $\beta = Q_{R\phi}/(R_{in}\Omega_{in})^2$ for the SRI as an α-like coefficient, this leads to

$$\alpha_{SS} = \beta \left(\frac{R_{in}}{H} \right)^2 \approx \beta \times 10^3, \tag{2.6}$$

with the so-called β viscosity (see Lynden-Bell & Pringle 1974; Huré, Richard & Zahn 2000). Here it is assumed that the SRI survives if the cylindrical container becomes larger in the radial direction, which is not yet clear.

3. Equations and numerical treatment

We use a code based on the non-isothermal hydrodynamic Fourier spectral element code described by Fournier *et al.* (2005) and Gellert, Rüdiger & Fournier (2007). With this approach we solve the three-dimensional hydrodynamic equations in Boussinesq approximation,

$$\partial_t \boldsymbol{U} + (\boldsymbol{U} \cdot \nabla)\boldsymbol{U} = -\nabla p + \nabla^2 \boldsymbol{U} + Gr \, T \, \hat{\boldsymbol{e}}_z, \tag{3.1}$$

$$\partial_t T + (\boldsymbol{U} \cdot \nabla) T = \frac{1}{Pr} \nabla^2 T, \tag{3.2}$$

$$\nabla \cdot \boldsymbol{U} = 0, \tag{3.3}$$

for an incompressible medium in a cylindrical annulus with inner radius R_{in} and outer radius R_{out}. Free parameters are the Grashof number

$$Gr = \frac{Ra}{Pr} = \frac{\alpha g \Delta T D^3}{\nu^2} \tag{3.4}$$

and the Prandtl number $Pr = \nu/\chi$. Here ν is the viscosity of the fluid and χ its thermal conductivity. $D = R_{out} - R_{in}$ is the gap width. The Reynolds number does not appear directly within the set of equations. It is defined, based on the inner cylinder's angular velocity, as $Re = \Omega_{in} R_{in} D/\nu$, with the gap width D (used as unit of length) and the angular velocity of the inner cylinder Ω_{in}. The unit of velocity is ν/D and the unit of time, i.e. the viscous time, is D^2/ν.

The solution is expanded in M Fourier modes in the azimuthal direction. This gives rise to a collection of meridional problems, each of which is solved using a Legendre spectral element method (see e.g. Deville, Fischer & Mund 2002). Between $M=8$ and $M=32$ Fourier modes are used. The polynomial order is varied between $N=8$ and $N=16$ with three elements in the radial direction. The number of elements in the axial direction depends on the height of the cylinder; the spatial resolution is the same as for the radial direction. With a semi-implicit approach consisting of second-order backward differentiation formula and the third-order Adams–Bashforth formula for the nonlinear forcing terms, time stepping is done with second-order accuracy.

At the inner and outer walls no heat–flux conditions are applied. In the axial direction, solid end caps with fixed temperatures T_0 and T_1 delimitate the cylindrical gap. The velocities of both the inner and outer cylinders are fixed to Ω_{in} and Ω_{out}, respectively. Stress-free conditions are applied on the end caps to prevent Ekman circulation that would result from solid end caps rotating with the angular velocity of the inner or outer cylinder. This restriction is not essential for the occurrence of the instability if the aspect ratio Γ is large enough. It simplifies the following analysis because data along the full cylinder height can be included.

As initial flow profile, we use the typical Couette profile

$$\Omega(R)=a+\frac{b}{R^2}, \tag{3.5}$$

with

$$a=\frac{\mu-\eta^2}{1-\eta^2}\Omega_{in}, \qquad b=\frac{1-\mu}{1-\eta^2}R_{in}^2\Omega_{in}, \tag{3.6}$$

the radius ratio $\eta=R_{in}/R_{out}$ and the ratio of angular velocities $\mu=\Omega_{out}/\Omega_{in}$. As initial temperature distribution, the linear static advection profile is applied.

Without stratification the critical Reynolds numbers for an infinite cylinder with $\eta=0.5$ is $Re_{crit}=68$ and $Re_{crit}=90$ for $\eta=0.78$. With our simulations we find $Re_{crit}=69$ and $Re_{crit}=91$, respectively, which we decided to be in good agreement.

4. Onset of instability

The SRI occurs as instability leading to non-axisymmetric flow patterns. After a linear growth phase, nonlinear interactions of the unstable modes occur resulting in a stable saturated state. The time the instability needs to evolve is around two viscous time scales D^2/ν or 120 system rotations, slightly depending on the Prandtl number. With $Pr=1$ it needs slightly more (150) rotations and for $Pr\geqslant 7$, nearly 100 rotations. After saturation a stationary state is reached where the flow pattern exhibits a drift compared to systems rotation. The growth rate of the instability is rather slow compared to other instabilities to produce (magnetohydrodynamic) turbulence like the magnetorotational instability (MRI) (see Balbus & Hawley 1991) or Tayler instability (TI) (see Tayler 1957; Rüdiger *et al.* 2007), where it is of the order of a few rotations. For both instabilities magnetic effects play an essential role. The SRI, even if slower, might be of comparable importance. As we will see in the following, it also leads to significant angular momentum transport. Moreover, stratification can suppress MRI or TI and hence it is the most efficient instability mechanism in environments with weak or very strong magnetic fields. MRI and TI are suppressed by strong magnetic fields. Also, in low-conducting environments like protostellar disks, where magnetic effects are unimportant, non-magnetic instabilities could be of high relevance.

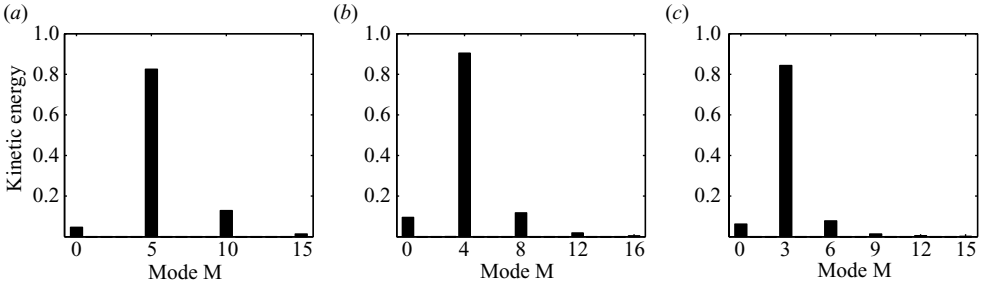

FIGURE 1. Histograms of Fourier modes for $Re = 500, Pr = 7$ in the small gap $\eta = 0.78$. (*a*) Plot for $Fr = 0.7$, (*b*) for $Fr = 1$ and (*c*) for $Fr = 1.4$. These show normalized total kinetic energy of the flow reduced by the driving due to the fixed cylinder rotation.

In our simulations we use two different gap sizes. The first one is a small gap with $\eta = 0.78$, which was also utilized in Shalybkov & Rüdiger (2005), and the second one is a wider gap with $\eta = 0.5$. Simulations are done with angular velocity ratios above the Rayleigh line. This means $\mu > 0.25$ for $\eta = 0.5$ and $\mu > 0.61$ for $\eta = 0.78$. Two special values, $\mu = 0.354$ for the wide gap and $\mu = 0.69$ for the small gap, are most interesting. These are the quasi-Keplerian profiles, i.e. inner and outer cylinders would rotate like planets after the Keplerian law $\sim R^{-3/2}$, between inner the profile differs slightly from a Keplerian. After the Rayleigh stability criterion $\partial_R(R^2\Omega)^2 > y0$ the configurations in our simulations are always hydrodynamically stable and the observed instability is due to the interplay between stratification and differential rotation.

4.1. *Wide gap*

The lowest critical Reynolds number for the onset of the instability is $Re = 285$ for $\eta = 0.5$, and thus a rather weak stratification supports the SRI as the most effective. The most obvious difference between both gap sizes is the dominating unstable mode. For the wide gap, it is always $m = 1$ in the observed parameter region $Re \leqslant 1000$, $1 \leqslant Pr \leqslant 10$ and $0.7 \leqslant Fr \leqslant 2$. All higher modes appear with gradual lower energy, where the step from mode m to $m + 1$ is between 10 % and 20 % of the higher mode. So the spectrum decreases very fast.

4.2. *Small gap*

In the case of the small gap, it is $m = 3$, $m = 4$ or $m = 5$ that becomes linear unstable and grows exponentially. The lowest critical Reynolds number here is $Re = 390$ for $Fr = 1.4$, again a weak stratification. When the unstable mode reaches a certain value, nonlinear effects appear and a wide range of modes become excited. After reaching the saturation level, the energy of the most unstable mode and of all harmonics stays constant, and all other modes decay slowly on the thermal time scale. The most unstable mode depends mainly on the stratification. For decreasing $Fr = 1.4, 1.0, 0.7$, the mode with the largest growth rate changes from $m = 3$ to $m = 4$ to $m = 5$. And it is also this mode (and its harmonics) that dominates the saturated state (see figures 1 and 2). For $Fr = 1.6$ it is $m = 2$ that becomes the largest non-axisymmetric mode and dominates the solution. For this rather low stratification one needs a larger Reynolds number of $Re = 1000$ to trigger the instability. So this solution is not directly comparable to all the other three cases with $Re = 500$. But the rule of decreasing m with the increase of Fr is still valid.

The Prandtl number within the range $1 \leqslant Pr \leqslant 10$ has no obvious influence on the type of solution and the most unstable mode. Moreover, neither a variation of

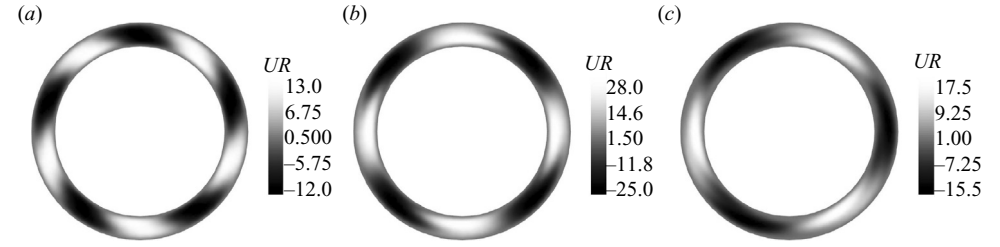

FIGURE 2. Contour plots of radial velocity component U_R in the mid-plane $z = \Gamma/2$ for $Re = 500$, $Pr = 7$ in the small gap $\eta = 0.78$. The plots are for (*a*) $Fr = 0.7$, $Fr = 1$ and (*b*) $Fr = 1.4$. The dominating Fourier mode is determined by the strength of the stratification.

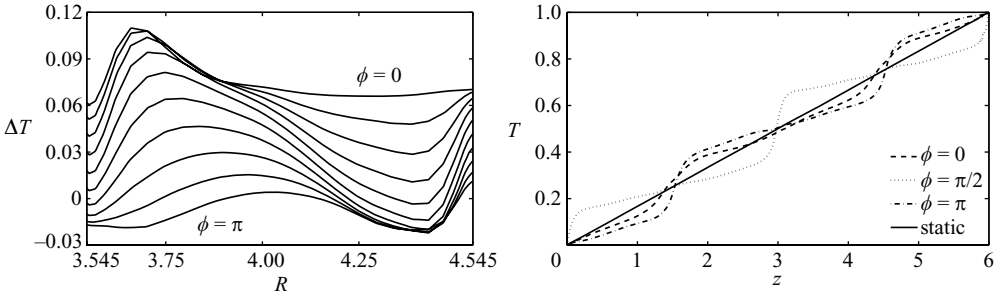

FIGURE 3. Radial and axial temperature profiles for $Re = 700$, $Pr = 7$, $Fr = 1.4$ in the small gap for several values of ϕ. Radial profiles are taken at half height and axial ones at the gap centre. Deviations from the linear static profile are around 15 %.

the Reynolds number (in the unstable region) nor a variation of the steepness of the rotation profile μ has an obvious effect. This is different from the results in Shalybkov & Rüdiger (2005), where μ and Re have a clear effect on the stability of the several modes. Either the lines of marginal stability for the modes are so close to each other that a distinction in the nonlinear simulations is impossible or the behaviour changes remarkably when the stratification is increased further. The lowest Froude number reachable in the nonlinear simulations is $Fr = 0.7$ and the linear analysis uses a value of $Fr = 0.5$. Low Fr is more demanding because Ra increases quadratically with Fr, and also Re needs to be larger and limits the accessible parameter space. Another aspect is in agreement with the linear analysis. For flat profiles ($\mu = 0.72$) we cannot find an instability for $\eta = 0.78$ and $Re \leqslant 1000$, which is the maximum Reynolds number we can reach in our simulations. Thus, SRI feeds from a good balance between stratification and rotation with a strong enough shear. The deviation from the linear static temperature profile is shown in figure 3. For a Reynolds number 1.5 times the critical one, it differs significantly by around 15 % from the linear profile. This effect becomes larger with increasing Re and vanishes near the onset of the stability.

5. Angular momentum transport

As shown in § 4, the variety of flow pattern is larger for the small gap container and might be a good choice for a laboratory experiment. Regarding angular momentum transport and its measurement, a wider gap is favourable as we demonstrate in the following. Further aspects of an experimental realization is dealt in § 6.

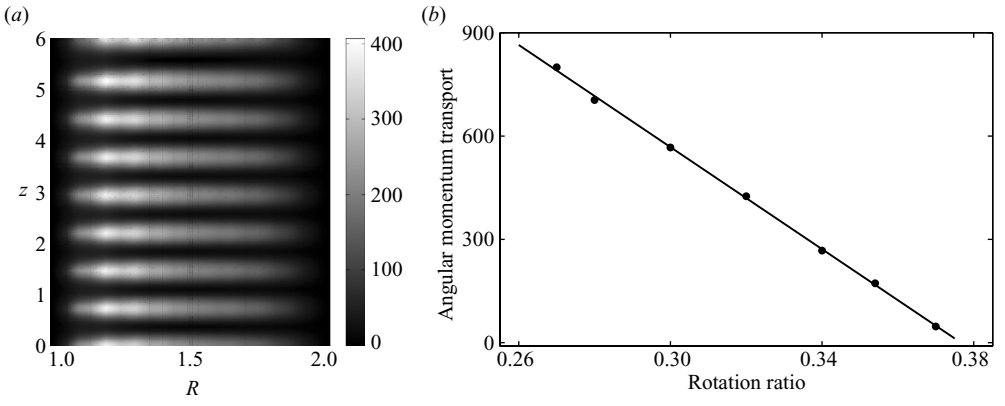

FIGURE 4. Pattern of Reynolds stress $Q_{R\phi} = \langle U_R' U_\phi' \rangle$ (a) for $\mu = 0.32$ and its linear dependence on shear (b). Angular momentum is transported outwards. Belonging parameters are $Re = 450$, $Pr = 1$, $Fr = 1$ and $\eta = 0.5$.

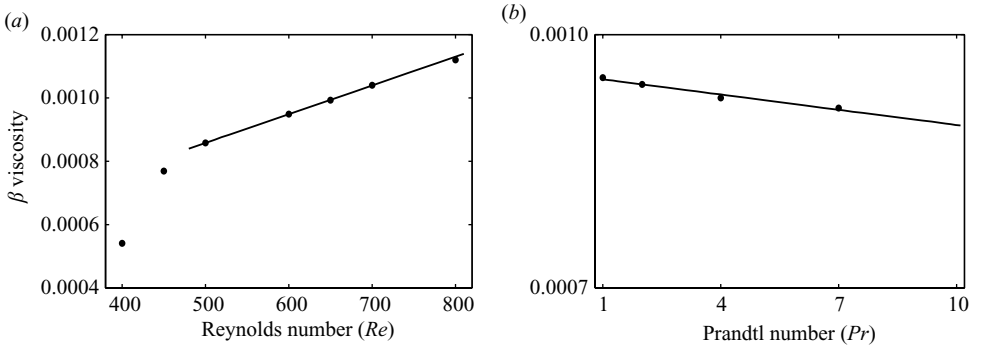

FIGURE 5. For $Fr = 1.4$, $\mu = 0.354$ and $\eta = 0.5$: (a) angular momentum transport in terms of the β viscosity at the gap centre ($R = 1.5$) and averaged along z for $Pr = 1$. For Re not in direct vicinity of the stability boundary, β depends linear on Re. (b) The weak dependence on the Prandtl number Pr is shown for $Re = 600$.

5.1. *Wide gap*

By using (2.3) the Reynolds stress $Q_{R\phi}$ is calculated for a fixed set of parameters. A typical pattern in the R–z plane is shown in figure 4 on the left. Angular momentum transport is always positive, i.e. directed outwards, with our configuration. The axial wavenumber varies between 4 and 12 for $\Gamma = 8$ depending mainly on the Froude number. Taking the value of $Q_{R\phi}$ in the gap centre ($R = 1.5$) averaged along z gives the linear dependence on μ, as shown in figure 4 on the right. Thus the angular momentum transport depends linearly on the shear.

An increase of Fr leads to decreased angular momentum transport because maintenance of the instability needs a stronger driving flow for increasing stratification. Whether there exists a maximum of $Q_{R\phi}$ for given Fr with increasing Re, as is the case for angular momentum transport due to the TI of a toroidal magnetic field (Gellert & Rüdiger 2008), is not easy to say. Within the accessible range of $Re \leqslant 1000$, $Q_{R\phi}$ increases linearly with Re and without indication of saturation (see figure 5a). A significant Prandtl number dependence cannot be found (figure 5b).

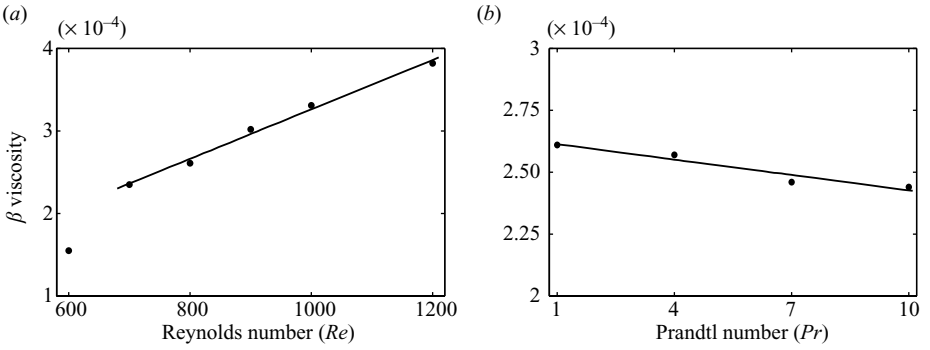

FIGURE 6. Same as in figure 5 but for the small gap with $\eta = 0.78$ and $Fr = 1.4$. It is for (*a*) $Pr = 1$ and (*b*) $Re = 800$.

The nearly vanishing influence of Pr might be a sign of the fact that it is not the convection-like temperature mixing that determines the SRI. This is only a secondary effect. The balance between centrifugal force and buoyancy is the crucial aspect. With $\chi \to 0$ and constant ν, the instability appears without qualitative change. This results in only a slight decrease in β. On the other hand, if both ν and χ are decreased (constant Pr and increasing Re), the β viscosity grows rapidly and linearly with Re, which means a scaling $Q_{R\phi} \propto \Omega^3$.

5.2. *Small gap*

Here the general behaviour is the same as for the wide gap. The different non-axisymmetric modes are not reflected in β. Compared with the small gap, the β viscosity is smaller by a factor of 4 but shows the same linear dependence on Re (see figure 6). The unimportant variation with the Prandtl number appears in the same way as for the wide gap for the observed Prandtl number range. This seems to be a very general behaviour and has also been reported for $Pr \geqslant 0.1$ by Dubrulle *et al.* (2005).

6. Suggestion for a laboratory experiment

Experiments to study the SRI till now use a stratification accomplished by a salt solution. Test probes along the depth help to keep the stratification linear as good as possible. Even if the unstable system would evolve deviations from the linear profile (and it would in the nonlinear regime as shown in figure 3), this is suppressed and the profile is forced to stay unchanged. This disadvantage can be avoided by using a temperature gradient to realize a strong enough stratification. Here the boundary conditions are well defined and it is a rather easy task to keep them constant in time. There exist many results, for instance from Rayleigh–Bénard experiments and other convective systems, of working with temperature gradients in the laboratory. That is why such a set-up is promising.

We show in the following of what size the TC system should be to reach appropriate stratifications and rotation speeds for water as working fluid. The Prandtl number of water is $Pr \approx 7$. For a possible set of parameters with $\eta = 0.5$, $Re = 500$, $\Gamma = 10$ and $Fr = 1.4$, one needs a Grashof number of $Gr = 1.3 \times 10^6$. This corresponds to a gap size of 6 cm for a temperature difference of 5 K or 9 cm for 2 K with water. Such dimensions for a TC system and the temperature difference are realizable in a laboratory. Figure 7 gives more details about dimensions, temperature differences

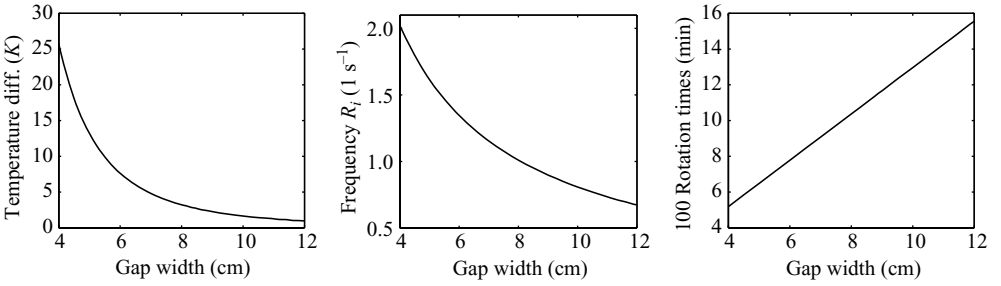

FIGURE 7. Needed temperature difference between top and bottom (*a*), rotation frequency of inner cylinder (*b*) and time to reach the saturation level (*c*) for $\eta = 0.5$, $Re = 800$, $Fr = 1.4$, $\Gamma = 10$ and $Pr = 7.16$ (water).

and rotation frequency of possible experiments with the same parameters but with $Re = 800$.

The crucial point seems to be the choice of the aspect ratio of the cylinders. On one hand one would like to extend the system to a high aspect ratio to limit perturbing effects from the end caps. On the other hand, increasing height linearly increases the required temperature difference, because it is the derivative $\mathrm{d}T/\mathrm{d}z$ that controls the instability and not the absolute value itself. Test simulations with solid end caps rotating with the angular velocity of the outer cylinder revealed that a smoothing of the pattern to axisymmetric structures near the top and bottom is inevitable, but it is the only effect if the aspect ratio is $\Gamma = 8$ or higher. Between 20 % and 80 % of the height the instability appeared in the same way as without solid end caps. Thus an aspect ratio of $\Gamma = 10$ might be an optimal choice for an experimental realization.

Beneath the instability itself, the transport of angular momentum should also be possible to measure. A scenario to do so could be the following. The whole system is mounted on a rotation table rotating with the angular velocity of the inner cylinder. The outer cylinder has its own drive to realize the relative angular velocity difference. The inner cylinder is connected to the table only by using thin wires. If the instability occurs, an additional torque acts on the inner cylinder and gives a measure for the β viscosity.

7. Discussion

We have shown fully nonlinear simulations of the SRI with temperature stratification in a cylindrical annulus. The stratification is stable, as well as the differentially rotating flow. Both lead to unstable non-axisymmetric modes. Depending on the gap width, these are the $m = 1$ or $m = 2/3/4/5$ modes in the investigated parameter range of rather weak stratification with Froude numbers around $Fr = 1$. Weak stratification results in the lowest critical Reynolds numbers for the onset of the SRI. On the other hand, the instability is influenced only slightly by the Prandtl number of the flow. The dominating mode m does not depend on Pr, but only on Fr. The time the SRI needs to evolve and reach a saturated state is of the order of 120 rotations or two times the viscous time scale. Thus the growth rate of the instability is rather slow compared to MRI and TI, where it is of the order of 10 rotations. For both instabilities magnetic effects play the essential role. The SRI, even if slower, might be of comparable importance when magnetic effects are rather unimportant or if stratification suppresses MRI or TI. Thus it might become the most efficient

instability mechanism in environments with weak or very strong magnetic fields or in low-conducting environments like protostellar disks. We indeed find that SRI could be a mechanism capable of transporting angular momentum. The normalized angular momentum transport in terms of the β viscosity is of the order of 10^{-3}, in terms of the α_{SS} for a thin disk around unity. This comparison with a thin disk assumes that SRI still occurs in such a flat disk, which is not possible to answer with our simulations at the moment. Nevertheless, the size of β and its linear growth with Re is a sign of significant influence of the SRI for angular momentum transport which might dominate over magnetic effects to produce turbulence in low-conducting environments. Besides astrophysical motivation, angular momentum transport and turbulent transport coefficients are also important for technical applications. In tradition of the idea of Couette to measure viscosity of a fluid, the presented experimental configuration could be used to measure the transport of angular momentum or the increase of viscosity in the laboratory. With water it needs a TC system with $\Gamma \approx 10$ and a gap width of 6 cm to observe the SRI with a temperature difference of 5 K between top and bottom. For Reynolds numbers around $Re = 1000$, the time the instability needs to grow and to saturate is around 25 min or 120 rotations at 0.5 Hz. All these conditions seem to be appropriate for an experiment.

The authors would like to thank Rainer Hollerbach for stimulating discussions.

REFERENCES

Balbus, S. & Hawley, J. F. 1991 A powerful local shear instability in weakly magnetized disks. I – Linear analysis; II – Nonlinear evolution. *Astrophys. J.* **376**, 214–233.

Boubnov, B. M., Gledzer, E. B. & Hopfinger, E. J. 1995 Stratified circular Couette flow: instability and flow regime. *J. Fluid Mech.* **292**, 333–358.

Boubnov, B. M., Gledzer, E. B., Hopfinger, E. J. & Orlandi, P. 1996 Layer formation and transitions in stratified circular Couette flow. *Dyn. Atmos. Oceans* **23**, 139–153.

Caton, F., Janiaud, B. & Hopfinger, E. J. 2000 Stability and bifurcations in stratified Taylor–Couette flow. *J. Fluid Mech.* **419**, 93–124.

Deville, M. O., Fischer, P. F. & Mund, E. H. 2002 *High Order Methods for Incompressible Fluid Flow*. Cambridge University Press.

Dubrulle, B., Marié, L., Normand, Ch., Richard, D., Hersant, F. & Zahn, J. P. 2005 A hydrodynamic shear instability in stratified disks. *Astron. Astrophys.* **429**, 1–13.

Fournier, A., Bunge, H.-P., Hollerbach, R. & Vilotte, J.-P. 2005 A Fourier-spectral element algorithm for thermal convection in rotating axisymmetric containers. *J. Comput. Phys.* **204**, 462–489.

Gellert, M. & Rüdiger, G. 2008 Toroidal field instability and eddy viscosity in Taylor–Couette flows. *Astron. Nachr.* **329**, 709–713.

Gellert, M., Rüdiger, G. & Fournier, A. 2007 Energy distribution in nonaxisymmetric magnetic Taylor–Couette flow. *Astron. Nachr.* **328**, 1162–1165.

Huré, J.-M., Richard, D. & Zahn, J.-P. 2001 Accretion discs models with the β-viscosity prescription derived from laboratory experiments. *Astron. Astrophys.* **367**, 1087–1094.

Le Bars, M. & Le Gal, P. 2006 Experimental analysis of the stratorotational instability in a cylindrical Couette flow. *Phys. Rev. Lett.* **99**, id. 064502.

Lynden-Bell, D. & Pringle, J. E. 1974 The evolution of viscous discs and the origin of the nebular variables. *Mon. Not. R. Astron. Soc.* **168,** 603–637.

Molemaker, M. J., McWilliams, J. C. & Yavneh, I. 2001 Instability and equilibration of centrifugally stable stratified Taylor–Couette flow. *Phys. Rev. Lett.* **86**, 5270–5273.

Rüdiger, G., Hollerbach, R., Schultz, M. & Elstner, D. 2007 Destabilisation of hydrodynamically stable rotation laws by azimuthal magnetic fields. *Mon. Not. R. Astron. Soc.* **377**, 1481–1487.

Rüdiger, G., & Shalybkov, D. 2008 Stratorotational instability in MHD Taylor–Couette flows. *Astron. Astrophys.*, accepted, arXiv: 0808.0577v1.

Shalybkov, D. & Rüdiger, G. 2005 Stability of density-stratified viscous Taylor–Couette flows. *Astron. Astrophys.* **438**, 411–417.

Shakura, N. I., & Sunyaev, R. A. 1973 Black holes in binary systems. Observational appearance. *Astron. Astrophys.* **24**, 337–355.

Tayler, R. J. 1957 Hydromagnetic instabilities of an ideally conducting fluid. *Proc. Phys. Soc.* B **70**, 31–48.

Thorpe, S. A. 1968 A method of producing a shear flow in a stratified fluid. *J. Fluid Mech.* **32**, 693–704.

Umurhan, O. M. 2006 On the stratorotational instability in the quasi-hydrostatic semi-geostrophic limit. *Mon. Not. R. Astron. Soc.* **365**, 85–100.

Withjack, E. M. & Chen, C. F. 1974 An experimental study of Couette instability of stratified fluids. *J. Fluid Mech.* **66**, 725–737.

Yavneh, I., McWilliams, J. C. & Molemaker, M. J. 2001 Non-axisymmetric instability of centrifugally stable stratified Taylor–Couette flow. *J. Fluid Mech.* **448**, 1–21.